Geoscientific
Model Development
Discussions

SILLi 1.0: A 1D Numerical Tool Quantifying the Thermal Effects of Sill Intrusions

3   *Karthik Iyer[1,2], Henrik Svensen[3] and Daniel W. Schmid[1,4]

4   *karthik.iyer@geomodsol.com

5   [1] GeoModelling Solutions GmbH, Zurich, Switzerland

6   [2] GEOMAR, Helmholtz Centre for Ocean Research, Kiel, Germany

7   [3] Centre for Earth Evolution and Dynamics, University of Oslo, Norway

8   [4] Physics of Geological Processes, University of Oslo, Norway

9

Abstract

11   Igneous intrusions in sedimentary basins may have a profound effect on the thermal structure and physical

12   properties of the hosting sedimentary rocks. These include mechanical effects such as deformation and uplift of

13   sedimentary layers, generation of overpressure, mineral reactions and porosity evolution, and fracturing and

14   vent formation following devolatilization reactions and the generation of CO_2 and CH_4. The gas generation and

15   subsequent migration and venting may have contributed to several of the past climatic changes such as the

16   end-Permian event and the Paleocene-Eocene Thermal Maximum. Additionally, the generation and expulsion of

17   hydrocarbons and cracking of pre-existing oil reservoirs around a hot magmatic intrusion is of significant

18   interest to the energy industry. In this paper, we present a user-friendly 1D FEM based tool, SILLi, which

19   calculates the thermal effects of sill intrusions on the enclosing sedimentary stratigraphy. The model is

20   accompanied by three case studies of sills emplaced in two different sedimentary basins, the Karoo Basin in

21   South Africa and the Vøring Basin offshore Norway. Input data for the model is the present-day well log or

22   sedimentary column with an Excel input file and includes rock parameters such as thermal conductivity, total

23   organic carbon (TOC) content, porosity, and latent heats. The model accounts for sedimentation and burial

24   based on a rate calculated by the sedimentary layer thickness and age. Erosion of the sedimentary column is

25 also included to account for realistic basin evolution. Multiple sills can be emplaced within the system with

26 varying ages. The emplacement of a sill occurs instantaneously. The model can be applied to volcanic

27 sedimentary basins occurring globally. The model output includes the thermal evolution of the sedimentary

28 column through time, and the changes that take place following sill emplacement such as TOC changes, thermal

29 maturity, and the amount of organic and carbonate-derived CO_2. The TOC and vitrinite results can be readily

30 benchmarked within the tool to present-day values measured within the sedimentary column. This allows the

31 user to determine the conditions required to obtain results that match observables and leads to a better

32 understanding of metamorphic processes in sedimentary basins.

33

1   Introduction

35 Volcanic processes can strongly influence the development of sedimentary basins associated with continental

36 margins. Magmatic bodies such as dikes and sills have a major impact on the thermal evolution of these

37 sedimentary basins. The short-term effects of igneous intrusions include deformation and uplift of the intruded

38 sediments, heating of the host rock, mineral reactions, generation of petroleum, boiling of pore fluids and

39 possible hydrothermal venting (Jamtveit et al., 2004; Malthe-Sorenssen et al., 2004; Svensen et al., 2004; Wang

40 et al., 2012b). Long-term effects include focused fluid flow, migration of hydrothermal and petroleum products,

41 formation of mechanically strong dolerite and hornfels in the contact aureole and differential compaction (Iyer

42 et al., 2013; Iyer et al., 2017; Kjoberg et al., 2017; Planke et al., 2005). This is of particular importance to

43 understanding the carbon cycle, as thermal stresses, besides those associated with burial, encountered by

44 organic matter in immature source rocks will determine the ultimate production and fate of the CO_2 and CH_4

45 generated. Vent structures are intimately associated with sill intrusions in sedimentary basins globally and are

46 thought to have been formed contemporaneously due to overpressure generated by pore-fluid boiling gas

47 generation during thermogenic breakdown of kerogen (Aarnes et al., 2015; Iyer et al., 2017; Jamtveit et al.,

48 2004). Methane and other gases generated during this process may have driven catastrophic climate change in

49 the geological past (Svensen and Jamtveit, 2010; Svensen et al., 2009). In order to understand these problems,

50 numerical models are widely used to reconstruct the thermal history of a basin where only a few of these

51 parameters are known.

Geoscientific
Model Development
Discussions

52 A number of analytical and numerical models have been developed that study the thermal effects of igneous

53 intrusions dating back to the early- and mid-1900's (Jaeger, 1964; Jaeger, 1957, 1959; Lovering, 1935).

54 Subsequent 1D and 2D models added additional complexity to the models by the addition of emplacement

55 mechanisms and timing, source rock maturation, hydrocarbon generation, latent heats of devolatilization and

56 maturation, fluid processes and overpressure generation (Aarnes et al., 2011a; Fjeldskaar et al., 2008;

57 Galushkin, 1997; Iyer et al., 2017; Monreal et al., 2009; Wang, 2012; Wang et al., 2010; Wang and Song, 2012;

58 Wang et al., 2012a). Contact metamorphic processes are well understood (e.g. (Aarnes et al., 2010; Jamtveit et

59 al., 1992; Tracy and Frost, 1991)), but many published papers do not take into account the basin history or the

60 variations in contact aureole thickness that arise from the type of measuring method that has been used. In

61 general, the contact metamorphic effects depend on 1) sill thickness (note that dikes cannot be directly

62 compared with sills), 2) sill emplacement temperature, 3) thermal gradient and emplacement depth (i.e.

63 temperature and background maturation), 4) emplacement history (instantaneous versus prolonged magma

64 flow), 5) host rock composition and characteristics (such as thermal conductivity, organic carbon content,

65 porosity, permeability) and 6) conductive versus advective cooling (e.g. (Aarnes et al., 2010; Galushkin, 1997;

66 Iyer et al., 2013; Iyer et al., 2017; Jaeger, 1964; Lovering, 1935; Wang, 2012)). In addition, the contact aureole

67 width depends on how aureoles are studied and measured. The aureole thickness depends on the proxy used,

68 including sonic velocity, density, mineralogy and mineral properties, magnetic susceptibility, total organic

69 carbon content, vitrinite reflectivity, color, porosity, or organic geochemistry. Note that these aureole thickness

70 proxies will not necessarily give the same result. Finally, the aureole thickness also depends on the proximity to

71 other sills emplaced at the same time (see Aarnes et al. (2011b) for a quantification).

72 In this paper we present a generic 1D thermal model, SILLi, which can be applied to studying the thermal effects

73 of sill intrusions in sedimentary basins globally. Besides heat transfer, the model also accounts for the

74 sequential deposition of sedimentary layers through time, erosion, latent heat effects and gas generation by

75 decarbonation reactions and organic matter maturation. The model results can be then easily compared to the

76 two most widely used aureole proxies in sedimentary rocks, vitrinite reflectance (VR) and total organic carbon

77 (TOC) data.

78

2   Model Input

80 The one dimensional, Finite Element Method (FEM) model numerically recreates the thermal effects of sill

81 emplacement in a sedimentary column. The model is written using MATLAB and requires version 2014b or

82 higher to run. The model input is specified in an Excel (*.xls) file and is read by the Matlab file, SILLi.m. The user

83 also specifies the model resolution with the igneous intrusions and sedimentary layers by giving the minimum

84 spacing (m) or the minimum number of points in the Matlab file. The measure that produces the highest

85 resolution is used. The Excel file is composed of seven tabs outlined below. If a previously calculated output file

86 is available for the input file, the program prompts the user to choose between loading the output file for

87 further analysis and performing a new calculation which overwrites the existing file.

88 For correct model use, the geological input needs to be based on either a borehole (with horizontal

89 stratigraphy) or an outcrop that is converted into a pseudo-borehole. If the case study is outcrop-based, a

90 pseudo-borehole stratigraphy should be constructed including the regional basin stratigraphy. Note that

91 sedimentary rocks present at higher stratigraphic levels elsewhere in the basin should be added to the erosion

92 history of the basin. Moreover, the sills (and samples) should be rotated back to horizontal if the stratigraphy

93 was tilted post sill emplacement. Using TOC and VR data from sedimentary rocks outside the immediate contact

94 aureoles will improve the model calibration.

95

2.1 Fluid

97 This tab contains three columns describing the fluid name, its density (kg/m^3) and its heat capacity (J/kg/K).

98

2.2 Lithology

100 This tab contains the data required for the model to build the present-day sedimentary column. The various

101 columns detail the name of the sedimentary layer (character only) and various material properties such as

102 density (kg/m^3), heat capacity (J/kg/K), porosity (fraction), thermal conductivity (W/m/K), initial TOC content

103 (wt%) and latent heats of organic maturation and dehydration (kJ/kg). Information regarding the kind of

104 carbonate contained in the sedimentary layer can be given in the last column if decarbonation reactions are

105 considered. The mineral constitution of the carbonate can be chosen as marl (1), dolomite (2) or

106 dolomite/evaporite mix (3). A zero (0) is entered in this column if decarbonation reactions are not required. The

107 lithology tab also contains columns where the present-day top depth (m) and age (Ma) of each layer can be

108 given which determine the depositional sequence and sedimentation rate for the layer (see Section 3.1). Note

109 that the ages of the sedimentary must be unique. A hypothetical basement is added 10 m below the deepest

110 sedimentary layer top depth or 300 m below the bottom of the deepest sill intrusion, whichever is deeper.

111

2.3 Erosion

113 This tab is similar to the lithology tab and contains information on eroded layers. Additional columns in this tab

114 contain information regarding the erosion timing (Ma) and the thickness of the eroded layer (m). Note that the

115 top depth of the eroded layer must coincide with the top of a sedimentary layer in the lithology tab. If part of

116 sedimentary layer is indeed eroded before deposition continues (i.e. the eroded layer lay inside a deposited

117 layer), the layer needs to be considered as unique layers separated by the eroded layer. Multiple eroded layers

118 can have the same top depths provided that older layers with the same top depth are eroded first. Similarly,

119 eroded layers have to be eroded first prior to deposition of younger layers. The ages of the eroded layers

120 cannot coincide with other layers.

121

2.4 Sills

123 This tab contains information necessary for the emplacement of sill intrusions. The top depth (m) and thickness

124 (m) of the sill constrain the geometry of the intrusion. Additional information includes the time of emplacement

125 (Ma), emplacement temperature (°C), melt and solid densities (kg/m³), melt and solid heat capacities (J/kg/K),

126 thermal conductivity (W/m/K), solidus and liquidus temperatures of the magma (°C) and the latent heat of

127 crystallization (kJ/kg). The emplacement of the intrusion is assumed to be instantaneous. Note that the top

128 depth of the sill cannot be the same as the top depth of a sedimentary layer. On the same note, the top depth

129 of a sedimentary layer cannot be inside a sill intrusion. Emplacement ages cannot exactly coincide with layer

130 ages.

Geoscientific
Model Development
Discussions

131

2.5   Temperature Data

This tab contains temperature data (°C) vs. depth (m) for the sedimentary column. The data in this tab is used to construct a geothermal gradient by using the best linear fit and therefore needs to contain at least two data points. Additionally, the first data point must coincide with the column top describing the surface temperature.

136

2.6   Vitrinite Data (Optional)

This tab contains present day vitrinite reflectance data presented in depth (m) and VR values (%Ro). Standard deviation of the values when available can be included. This data is used for comparison of the modelled VR values to observations. This tab can be left blank if no information is available.

141

2.7   TOC Data (Optional)

This tab contains present day TOC content data (wt%) vs. depth (m) measured in the sedimentary column which is used to compare to the model results. This tab can be left blank if no information is available.

145

3   Method

3.1   Sediment Deposition and Erosion

Each sedimentary layer, including the eroded layers, is deposited sequentially in time based on the depositional age. The rate of sedimentation for each layer is determined by the thickness of the layer and the difference in time between its top age and that of the layer deposited before it. Erosional layers in the sedimentary column are deposited in the same way as other layers. Erosion of the entire layer occurs within a single step at the specified erosion age. The temperature boundary conditions are accordingly adjusted for the height of the new sedimentary column. Note that the bottom boundary is extended to 5 times the thickness of the bottommost sill if that sill is close to or at the bottom boundary in order to remove boundary effects.

155

3.2 Thermal Diffusion

The thermal solver computes the temperature within the deposited sedimentary column by applying fixed temperatures at the top and bottom at every step which are calculated from the prescribed geotherm (see Section 2.5) and the energy diffusion equation,

$$\left[\phi \rho_f c_{pf} + (1-\phi) \rho_r c_{peff} \right] \frac{\partial T}{\partial t} = \nabla \cdot (\kappa \nabla T) \tag{1}$$

Table 1 contains the definitions of all the notations used in the manuscript. The effective rock heat capacity accounts for the latent heat of fusion in the crystallizing parts of the sill between the solidus (T_S) and liquidus (T_L) temperature of the magma (e.g. (Galushkin, 1997))

$$
\begin{aligned}
c_{peff} &= c_{pm} \left[1 + \frac{L_c}{(T_L - T_S) c_{pm}} \right] \text{ if } [T_S < T < T_L] \\
c_{peff} &= c_{pr} \qquad\qquad\qquad \text{ if } [T_S > T]
\end{aligned}
\tag{2}
$$

Sills are emplaced instantaneously at the specified time and temperature within the sedimentary column. The emplacement of multiple sills in the same step is possible. The time-steps used for thermal diffusion after sill emplacement are automatically calculated based on the sill thickness and the characteristic time required for thermal diffusion. The time step is initially small in order to accurately resolve the thermal evolution of the contact aureole around the sill and is gradually increased once the energy released by the cooling sill is dissipated.

Dehydration reactions in the host rock are implemented by modifying the thermal diffusion equation when temperatures of the sediments increase within a certain range (Galushkin, 1997; Wang, 2012)

$$\left[\phi \rho_f c_{pf} + (1-\phi) \rho_r c_{peff} \right] \frac{\partial T}{\partial t} = \nabla \cdot (\kappa \nabla T) - H \tag{3}$$

Geoscientific
Model Development
Discussions

174

$$H = \frac{(1-\varphi)\,\rho_r L_d}{T_{d1} - T_{d2}} \frac{\partial T}{\partial t}$$

(4)

Symbol	Description	Units
A	Frequency factor	s^{-1}
c_{peff}	Effective rock heat capacity	$J\ kg^{-1}\ K^{-1}$
c_{pf}	Fluid heat capacity	$J\ kg^{-1}\ K^{-1}$
c_{pr}	Rock heat capacity	$J\ kg^{-1}\ K^{-1}$
E	Activation energy	$KJ\ mol^{-1}$
f	Stoichiometric factor	
F	Reaction extent	
g	Gravitational acceleration	$m\ s^{-2}$
i	Reactive component	
L_c	Latent heat of crystallization	$KJ\ kg^{-1}$
m_{CO_2}	Carbon to CO_2 conversion factor	3.66
P_{atm}	Atmospheric pressure	10^5 Pa
P_{H2O}	Hydrostatic pressure	Pa
R_{CO_2}	Rate of CO_2 generation	$kg\ m^{-3}\ s^{-1}$
R_{om}	Rate of organic matter degradation	$kg\ m^{-3}\ s^{-1}$
t	Time	s
T_L	Liquidus temperature	°C
T_S	Solidus temperature	°C
T	Temperature	°C
T_{d2} - T_{d1}	Temperature range for dehydration reactions (Galushkin, 1997)	350-650 °C
w	Amount of reactive component	Fraction
Z	Depth	km
ϕ	Rock porosity	Fraction

Geoscientific
Model Development
Discussions

κ	Conductivity	W m^{-1} K^{-1}
ρ_f	Fluid density	kg m^{-3}
ρ_r	Rock density	kg m^{-3}

Table 1. Definition of symbols used in the model.

3.3 Thermal Maturation of Organic Matter

Vitrinite reflectance is a widely used indicator of thermal maturity and can be readily measured in the field. One of the most common methods used to calculate the thermal maturity of the source rock is the EASY%Ro method put forward by Sweeney and Burnham (1990). This model uses 20 parallel Arrhenius-type of first order reactions to describe the complex process of kerogen breakdown due to temperature increase. The reaction for the ith component is given by

$$\frac{dw_i}{dt} = -w_i A \exp\left[-\frac{E_i}{RT^t}\right] \tag{5}$$

where w_i is the amount of material for component i, E_i is the activation energy for the given reaction and T^t is time-dependent temperature.

The total amount of material reacted is obtained by summing up the individual reactions

$$\frac{dw}{dt} = \sum_i \frac{dw_i}{dt} \tag{6}$$

The fraction of reactant converted is

$$F = 1 - \frac{w}{w_0} = 1 - \sum_i f_i \left(\frac{w_i}{w_{0i}}\right) \tag{7}$$

from which the vitrinite reflectance can be readily calculated by

Geoscientific
Model Development
Discussions

191
$$\% Ro = \exp\left(-1.6 + 3.7F\right) \tag{8}$$

192 The amount of TOC that has reacted for any given time can be calculated by

193
$$\mathrm{TOC}(t) = \mathrm{TOC}_o F(t) \tag{9}$$

194 and the rate of organic matter degradation by

195
$$R_{om} = \left(1-\phi\right)\rho_r \frac{\partial \mathrm{TOC}}{\partial t} \tag{10}$$

196 The maximum amount of TOC that can be reacted by this method is 85% of the initial total. Note that in the
197 inner part of the contact aureole close the sill, data shows that all of the organic matter has been reacted or
198 removed (eg. LA1/68 in section 5.2.2). We assume that all of the hydrocarbons released during thermal
199 degradation are converted into carbon dioxide. The amount of organic carbon dioxide generated (R_{CO2}) for a
200 time step is given by

201
$$R_{CO_2} = R_{om} m_{CO_2} \tag{11}$$

202 where m_{CO2} is a stoichiometric conversion factor (3.67) to transform carbon into carbon dioxide. Note that
203 metamorphism of sedimentary rocks will generate CH_4 (e.g., (Aarnes et al., 2010; Iyer et al., 2017)), but in our
204 model the reacted carbon is recalculated to CO_2. If needed, the CO_2 model output can be easily converted to
205 either C or CH_4.

206 The latent heat of organic maturation is accounted for in the energy equation

207
$$\left[\phi\rho_f c_{pf} + \left(1-\phi\right)\rho_r c_{peff}\right]\frac{\partial T}{\partial t} = \nabla\cdot\left(\kappa\nabla T\right) - H - L_{om}R_{om} \tag{12}$$

208

3.4 Mineral Decarbonation

210 Carbonate minerals undergo decarbonation reactions as they are heated to high temperatures. This results in
211 mineral transformations and the release of inorganic carbon dioxide which may significantly add to the CO_2

Geoscientific
Model Development
Discussions

budget associated with igneous intrusions. The amount of inorganic CO_2 liberated during metamorphic transformation over a range of temperature and fluid pressure for marl, dolomite and dolomite/evaporite mixture is pre-computed as a phase diagram using Perple_X (Connolly and Petrini, 2002) (Figure 1). The model evaluates the total amount of inorganic CO_2 liberated by carbonate layers based on the temperature and pressure evolution of the layer through time within the phase diagrams. Fluid pressure within the sedimentary column is calculated by integrating the rock density over depth in addition to atmospheric pressure:

$$P_{H_2O} = P_{atm} + \int_{Z_{min}}^{Z_{max}} \rho_f \vec{g}$$

(13)
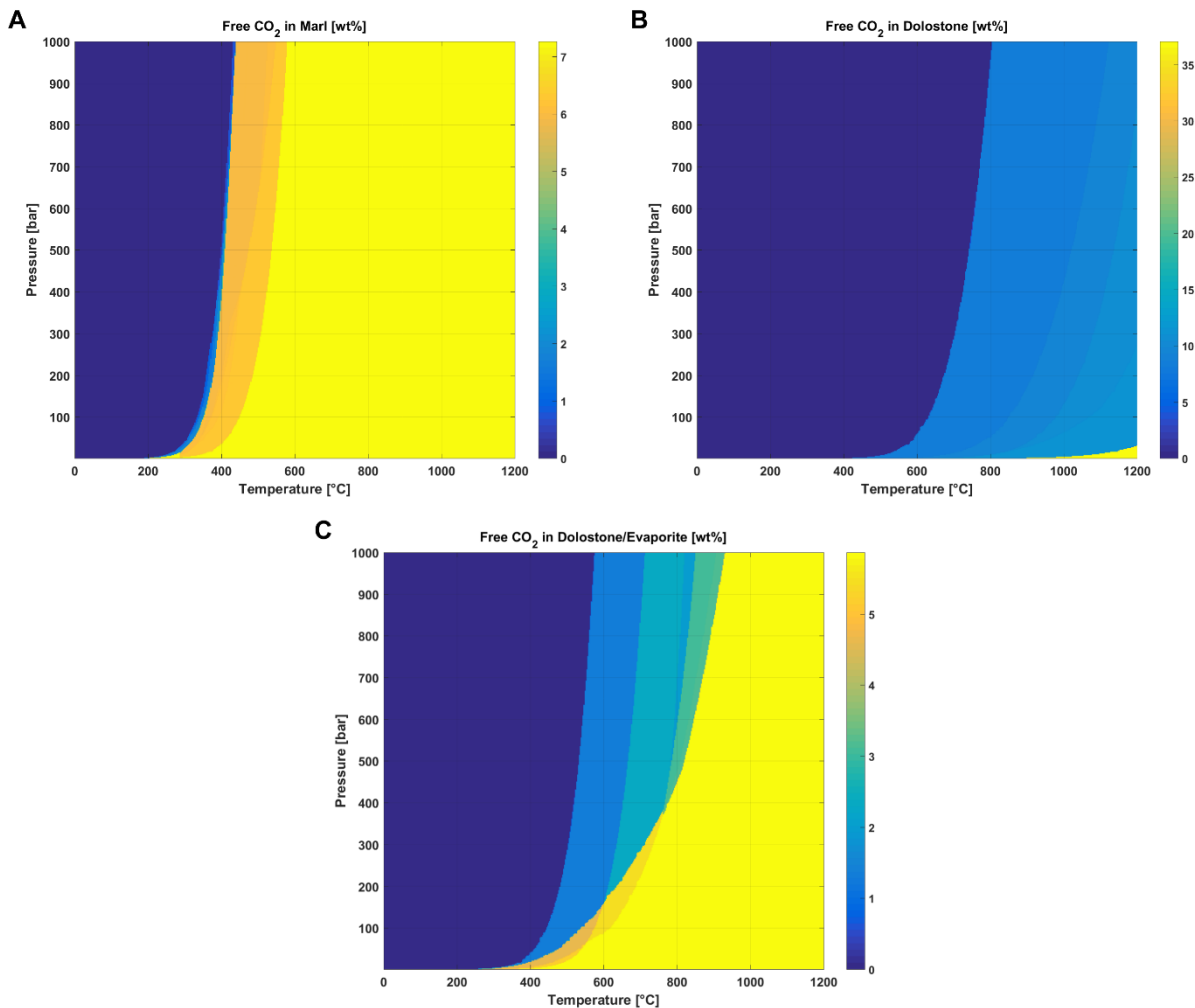
220 *Figure 1. Phase diagrams generated by Perple_X showing the amounts of inorganic CO_2 liberated with respect to*

221 *temperature and pressure for marl (A), dolostone (B) and dolostone/evaporite (C).*

3.5 Model Mesh and Time-Stepping

The entire sedimentary column including the eroded layers and igneous intrusions is reconstructed and the column nodes and elements for the FEM model are generated using the user-specified resolution. The nodes are initially collapsed onto each other in depth. Each sedimentary node is assigned a time during which it is expanded (or deposited) within the sedimentary column based on the layer age and its thickness. All of the elements and nodes associated with each igneous intrusion are expanded simultaneously during the corresponding emplacement time. Eroded layers are removed in a single time step specified by the erosion age and the corresponding nodes are collapsed. In order to correctly capture thermal diffusion across the large thermal gradient adjacent to a hot intrusion, the time step is initially very small and exponentially increases during the heating period after sill emplacement and before the next depositional event. The heating period of the sill, over which the exponential time sub-stepping is used, is analytically determined from the characteristic diffusion time for the sill thickness (Jaeger, 1959).

3.6 Model Limitations

- The model is one-dimensional and will therefore not resolve thermal effects that would require a full 3D model.
- The model does not account for advective transport of heat through the system by fluids. However, previous models have shown that this process would be dominant only in high permeability systems or at the sill edges/tips in low permeability systems (Iyer et al., 2013; Iyer et al., 2017). Therefore, the model presented in this manuscript works well for relatively low permeability systems with shales, mudstone etc. and when the sedimentary column passes through the sill interior away from the edges.
- The model does not account for other mineral reactions in the contact aureole besides decarbonation of carbonates. The various mineral reactions possible in the contact aureole can be implemented as an add-on module to the model if needed.
- The model assumes that TOC conversion in all types of sedimentary rocks can be estimated by using the EASY%Ro method with a maximum conversion value of 85%. Although, this is a good first approximation, it cannot account for the complete loss of carbon in zones very close to the sill-host rock interface which would result in an underestimation of the released gases (Svensen et al., 2015). On the

250 other hand, the provenance of the sedimentary rock can also significantly affect how kerogen present in
251 organic matter reacts to form hydrocarbons which may result in a reduction in the amount of
252 convertible organic matter due to the presence of inert kerogen (Iyer et al., 2017; Pepper and Corvi,
253 1995).

254

4   Model Output

256 The model input and results are presented with the help of a GUI (Section 4.6). Model data are written out as a

257 single .mat (Matlab data) file in the same directory as the user-defined path for the input Excel file and with the

258 same filename. The file contains five 'struct' variables of which three contain input information (rock, sill and

259 welldata) and the other two contain model results (result and release). The structure of the variables are

260 described below.

261

4.1   Struct Variable: rock

263 This variable contains input information on the sedimentary layers in the column including the eroded layers.

264 The information is saved as variables given in Table 2 and is sorted according to their top depths. Note that top

265 depths are corrected for the eroded layers that are also included.

Variable Name	Description
Name	User-defined names of all the sedimentary layers in the column.
num	Total number of deposited sedimentary layers.
top	Top depth of the shallowest sedimentary layer.
bot	Top depth of the deepest sedimentary layer.
Tops	Top depths of sedimentary layers.
Ages	Ages of sedimentary layers.
Rho	Density of sedimentary layers.
Cp	Heat capacity of sedimentary layers.
Phi	Porosity of sedimentary layers.

K	Thermal conductivity of sedimentary layers.
Toc	TOC content of sedimentary layers.
Lm	Latent heat of maturation of sedimentary layers.
Ld	Latent heat of dehydration of sedimentary layers.
Carb	Carbonate layer identifier (0-3).
Ero_t	Erosion age of sedimentary layers (NaN if layer is not eroded).
Ero_thick	Eroded thickness of sedimentary layers (NaN if layer is not eroded).
Ero_tops	Top depths of the eroded layers only.

266   *Table 2. List of variables in 'rock' struct variable of the output file.*

267

4.2   Struct Variable: sill

269   This variable contains input information on sill intrusions in the column. The information is saved as variables

270   given in Table 3 and is sorted according to their top depths.

Variable Name	**Description**
num	Total number of sill intrusions.
Tops	Top depths of sill intrusions.
E_time	Emplacement ages of sill intrusions.
E_temp	Emplacement temperatures of sill intrusions.
Rhom	Melt density of sill intrusions.
Cpm	Melt heat capacity of sill intrusions.
Rhos	Solid density of sill intrusions.
Cps	Solid heat capacity of sill intrusions.
K	Thermal conductivity of sedimentary layers.
Sol	Solidus of melt in sill intrusions.
Liq	Liquidus of melt in sill intrusions.
Ld	Latent heat of crystallization of melt in sill intrusions.

271 *Table 3. List of variables in 'sill' struct variable of the output file.*

272

4.3   Struct Variable: welldata

274 This variable contains input information on measured TOC, VR and temperature data for the sedimentary

275 column. The information is saved as variables given in Table 4.

Variable Name	Description
TOC	Measured TOC data vs. depth.
VR	Measured VR data vs. depth.
T	Measured temperature data vs. depth.

276 *Table 4. List of variables in 'welldata' struct variable of the output file.*

277

4.4   Struct Variable: result

279 This variable contains the model results which are saved for every time step when applicable, i.e. variables that

280 change over time have rows corresponding to the element or node number (depending on where they are

281 defined) and columns corresponding to the time step number. The information is saved as variables given in

282 Table 5.

Variable Name	Description (Rows x Columns)
nel	Number of elements in the model (1 x 1)
nnod	Number of nodes in the model (1 x 1)
Gcoord_c	Depth of element centers (1 x no. of elements)
Ind	Internal nodal indexing of sedimentary layers and intrusions (no. of nodes x 1). Intrusions are negatively indexed.
Ind_nel	Internal element indexing of sedimentary layers and intrusions (no. of elements x 1). Intrusions are negatively indexed.
Ind_carb	Nodal indexing of carbonate layers (0-3) (no. of nodes x 1).

Gcoord	Depth of nodes (no. of nodes x no. of time steps).
Temp	Nodal temperature (no. of nodes x no. of time steps).
Pres	Nodal hydrostatic pressure (no. of nodes x no. of time steps).
Toc	Remaining Toc content at nodes (no. of nodes x no. of time steps).
CO2_org	Organic carbon dioxide generated at nodes (no. of nodes x no. of time steps).
Ro	VR at nodes (no. of nodes x no. of time steps).
Tmax	Maximum temperature experienced at nodes (no. of nodes x no. of time steps).
Active	Binary index of 'deposited/expanded' nodes (no. of nodes x no. of time steps).
CO2_release	Inorganic carbon dioxide generated at nodes (no. of nodes x no. of time steps).
Time	Year count for time step (no. of time steps x 1).

283   Table 5. List of variables in 'result' struct variable of the output file.

284

4.5 Struct Variable: release

286   This variable contains the amounts of CO_2 released for every time step normalized to rock volume. The

287   information is saved as variables given in Table 6.

Variable Name	Description (Rows x Columns)
CO2_org	Organic carbon dioxide generated in elements normalized to rock volume (no. of elements x no. of time steps).
CO2_rel	Inorganic carbon dioxide generated in elements normalized to rock volume (no. of elements x no. of time steps).

288   Table 6. List of variables in 'release' struct variable of the output file.

289

4.6 Output Graphical User Interface (GUI)

291   The GUI presented during and after the model run contains three tabs containing graphical representations of

292   the input data, time evolution of model results and CO_2 release through time. An explanation of the tabs is

293   given below using a hypothetical test case consisting of a sedimentary column with two sill intrusions and three

294   eroded layers.

4.6.1   Input Tab

296   The left-most subplot of the input tab contains the reconstructed sedimentary column where the layers are

297   colored according to their depositional age (http://www.stratigraphy.org/index.php/ics-chart-timescale) (Figure

298   2). The sedimentary column also contains eroded layers (hatched) and sill intrusions (speckled). The name and

299   depositional age of a layer can be found by right-clicking the layer. The other subplots in the input tab contain

300   information on the density, porosity, initial TOC content and thermal conductivity of the sedimentary layers.

301   The values of these variables are plotted at the corresponding layer top depth.
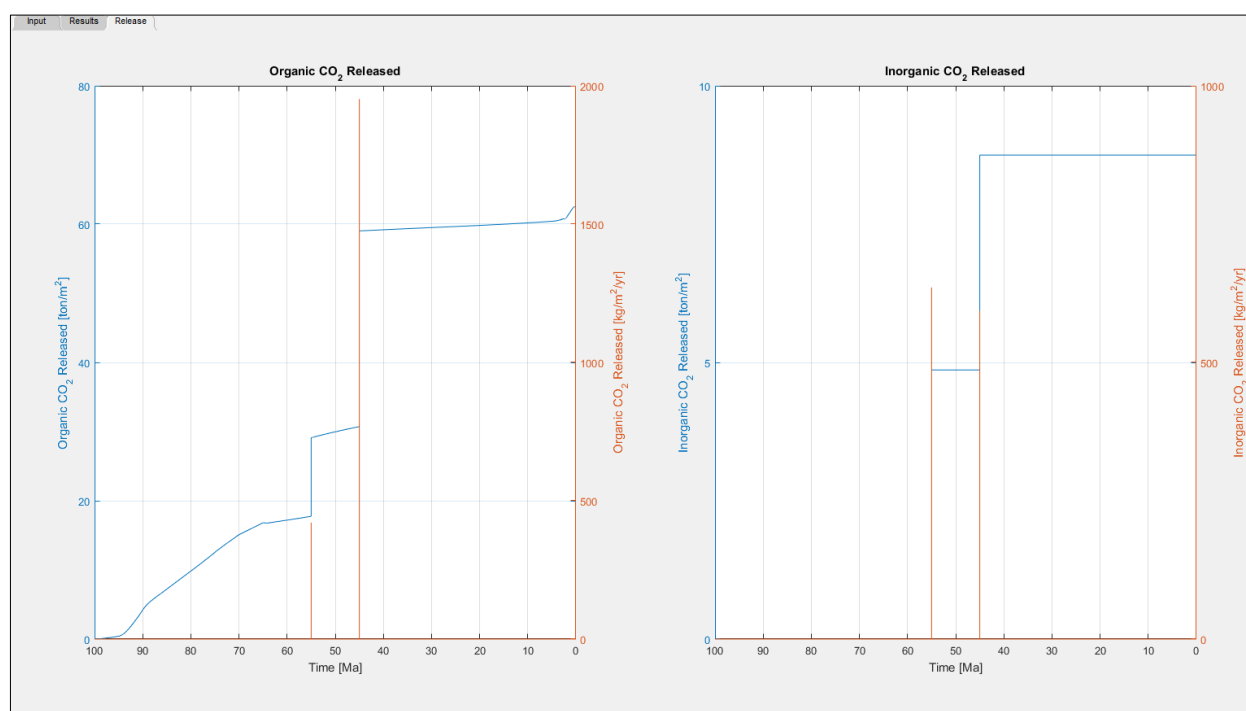

302
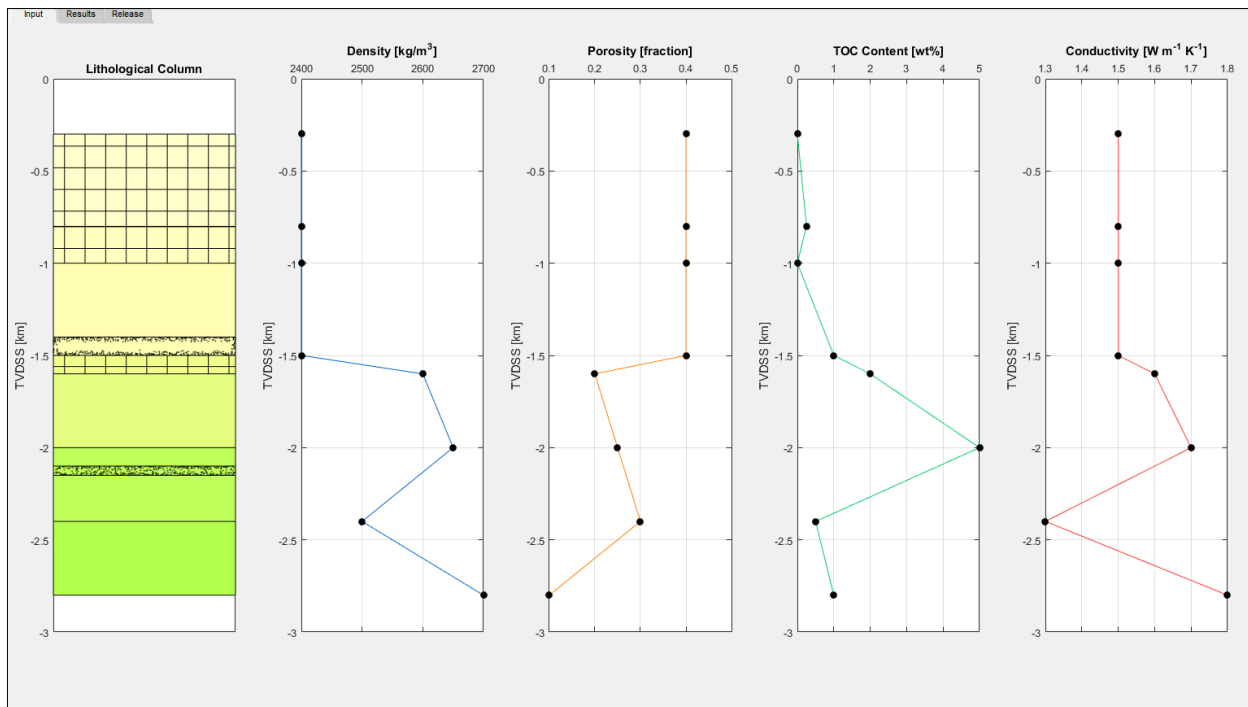
Figure 2. Snapshot of the input tab generated for a hypothetical sedimentary column with two sill intrusions and three eroded layers. Right-clicking a layer in the sedimentary column provides the name and depositional/erosional age of the layer.

4.6.2   Results Tab

306

307   The results tab consists of the evolution of temperature, vitrinite reflectance, TOC content, maximum

308   temperature, hydrostatic pressure, inorganic and organic CO_2 release within the sedimentary column over

309   simulated time (Figure 3). The evolution of these variables can be played or stepped through using the player

310   controls in the top left corner. Alternatively, the user can jump directly to the desired geological time by

311   inputting it in the player control. Note that this results in the plot jumping to the time-step nearest the desired

312   time input. Regions containing sill intrusions are highlighted in gray. Users can copy plot data at any time step

313   by right-clicking the curve.

314
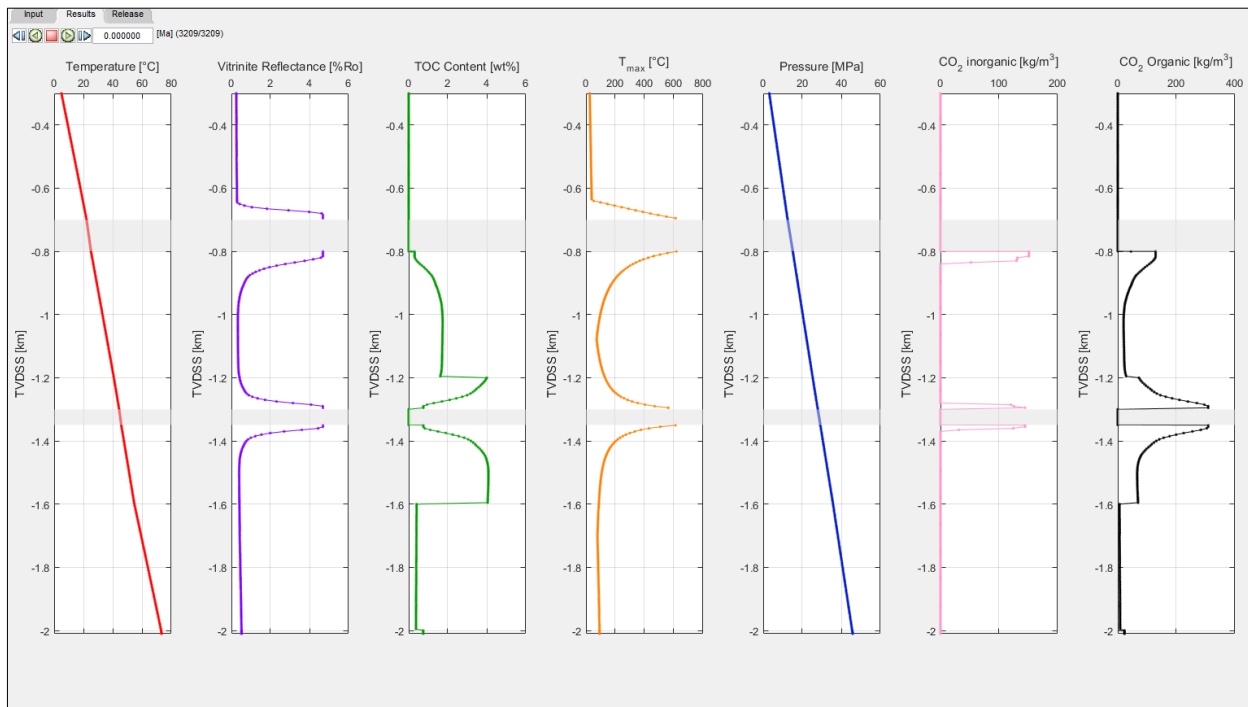
Figure 3. Snapshot of the results tab generated for a hypothetical sedimentary column with two sill intrusions
and three eroded layers. Right-clicking any curve allows the user to copy curve data.

4.6.3   Release Tab

318   The release tab plots the cumulative and rates of release of organic and inorganic CO_2 due to heating of the

319   sedimentary layer by sill intrusions (Figure 4). The cumulative and release rates are summed over the entire

320   sedimentary column. The user can use the cumulative amount of gas released to easily upscale to basin scales

321   by multiplying the value by the area affected by sill intrusions. Users can copy plot data at any time step by

322   right-clicking the curve.

323

324   *Figure 4. Snapshot of the release tab generated for a hypothetical sedimentary column with two sill intrusions*

325   *and three eroded layers. Right-clicking any curve allows the user to copy curve data.*

326

5   Examples

328   The examples below are provided with the code and are used to benchmark observations to model results.

5.1 Utgard High

330   The Utgard sill complex is part of the North Atlantic Igneous Province (NAIP) in the Vøring and Møre Basins,

331   offshore Norway. This region underwent massive volcanic activity at the Paleocene-Eocene boundary around

332   ~55 Ma (Aarnes et al., 2015). The Utgard High borehole 6607/5-2 was drilled through two sills emplaced in the

333   Upper Cretaceous sedimentary layers. The drilled lithological column consists of nine layers with the oldest

334   being deposited 100 Ma (NPD Factpages, http://factpages.npd.no/factpages/) (Figure 5). For simplicity, the

335   material properties of the entire sedimentary column is set to constant values with the exception of TOC

336   content. TOC content of the Paleocene and Upper Cretaceous sedimentary layers are set to an initial value of

337   0.6 and 1.5 wt%, respectively. Carbonate and erosional layers are not considered. The modelled sedimentary

338   layers are sequentially deposited at the sedimentation rate calculated from the layer top ages. The two sills are

339   emplaced simultaneously within the Nise and Kvitnos Formations at 55 Ma at a temperature of 1150°C.

340   Sedimentary rocks around the emplaced sills are progressively heated as the sills cool. The vitrinite reflectance

341   values increase and the TOC content reduced by thermally degrading organic matter to form CO_2 (Figure 6).

342   Sedimentation after sill emplacement results in further burial and extension to produce the present-day

343   sedimentary column. Vitrinite reflectance and TOC data from the Norwegian Petroleum Directorate (NPD) and a

344   previous study (Aarnes et al., 2015) are used to benchmark the model and match very well with the modelled

345   results (Figure 7). Further information about the geological and model setting can be found in Aarnes et al.

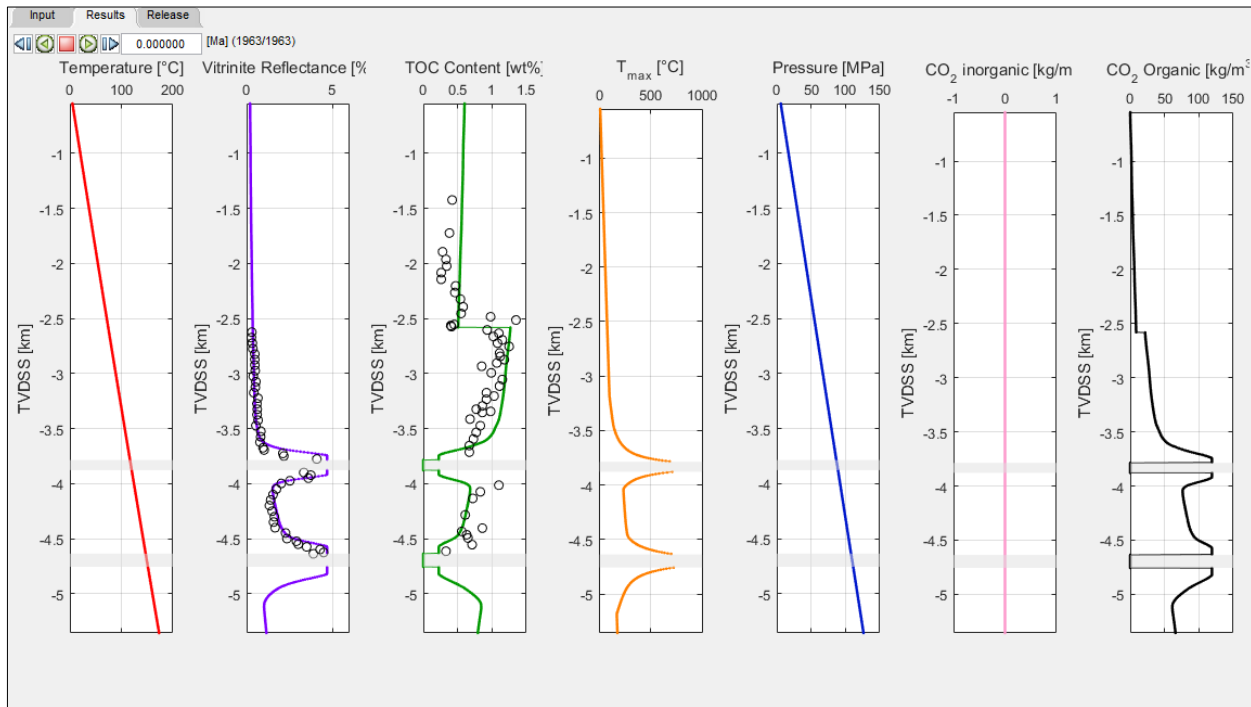346   (2015) and the input file '1d_sill_input_utgard.xlsx'.
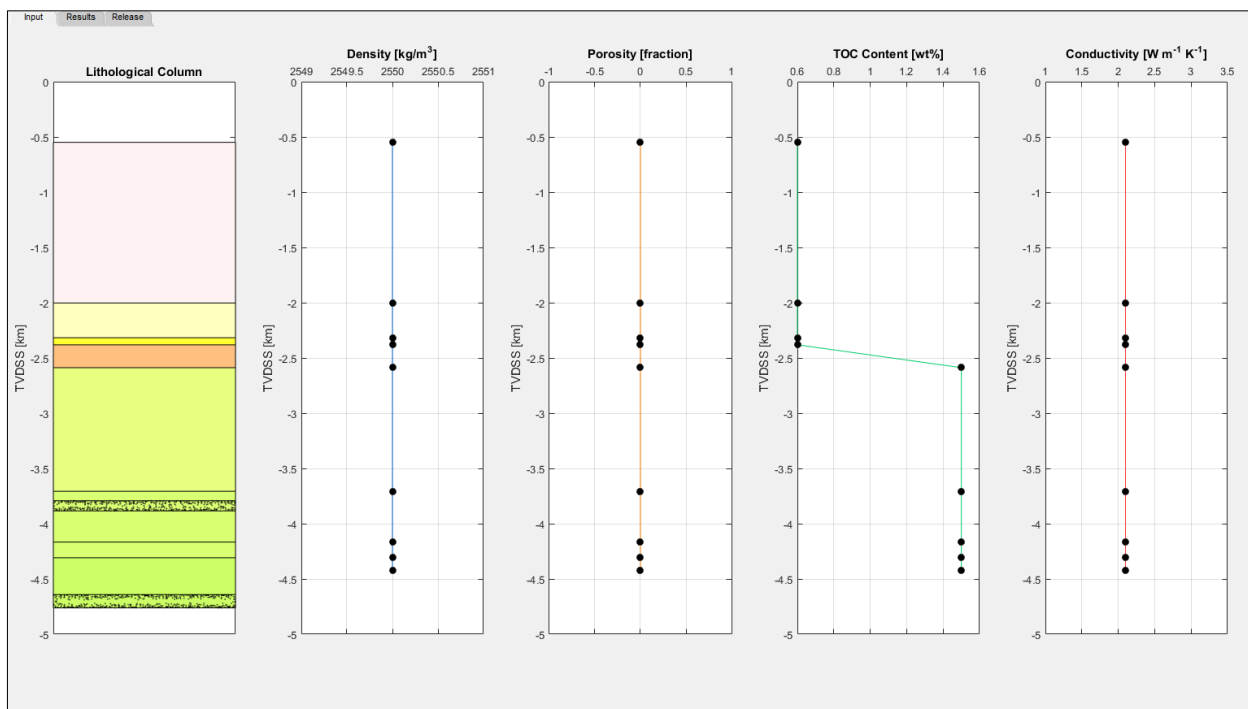
347

348   *Figure 5. Input tab for the Utgard High example.*

349
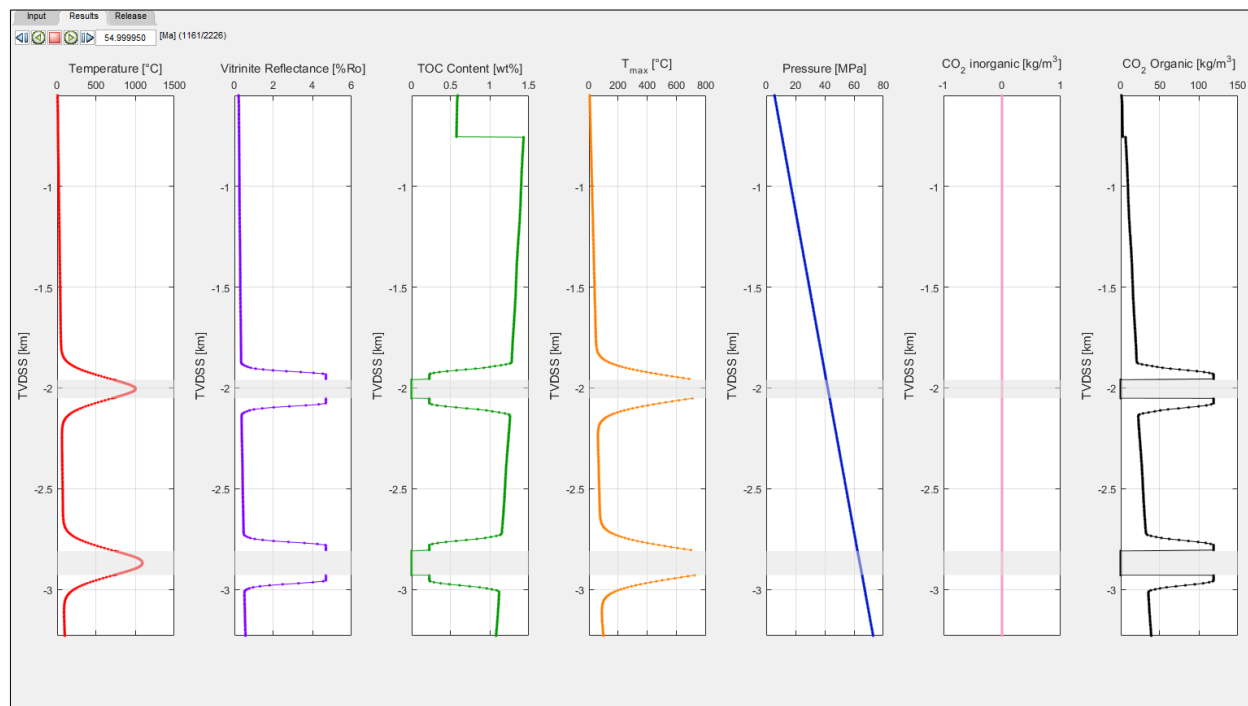
Figure 6. Results tab 50 years after the emplacement of sills at 55 Ma for the Utgard High example. Sediments

around the sills are heated and CO_2 is liberated as organic matter is thermally degraded.

350

351

352

Figure 7. Results tab at the end of simulation time for the Utgard High example. The present-day VR and TOC values (circles) show a good match with the model results.

5.2 Example 2

The Karoo Large igneous province was emplaced through the Karoo Basin in South Africa in the Early Jurassic. The basin contains sills and dykes of varying thickness (Chevallier and Woodford, 1999; du Toit, 1920; Svensen et al., 2015; Walker and Poldervaart, 1949) , emplaced at about 182.6 Ma (Svensen et al., 2012). The basin stratigraphy consists of the Upper Carboniferous to the Triassic Karoo Supergroup and is divided in five groups (the Dwyka, Ecca, Beaufort, Stormberg and Drakensberg groups) with a postulated maximum cumulative thickness of 12 km and a preserved maximum thickness of 5.5 km (Tankard et al., 2009). The depositional environments of the sediments range from marine and glacial (the Dwyka Group), marine to deltaic (the Ecca Group), to fluvial (the Beaufort Group) and finally eolian (the Stormberg Group) (Catuneanu et al., 1998). The Karoo Basin is overlain by 1.65 km of preserved volcanic rocks of the Drakensberg Group, consisting mainly of stacked basalt flows erupted in a continental and dry environment (e.g., (Duncan et al., 1984)). Several recent

22

Geoscientific
Model Development
Discussions

368   studies have been devoted to contact metamorphism of the organic-rich Ecca Group (Aarnes et al., 2011b;

369   Moorcroft and Tonnelier, 2016) and the possible consequences of thermogenic methane venting on the Early

370   Jurassic climate (Svensen et al., 2007; Svensen et al., 2015). Here we present two borehole cases from the

371   central (borehole KL1/78) and eastern (borehole LA1/68) parts of the basin previously studied and modelled by

372   Aarnes et al. (2011b) and Svensen et al. (2015), respectively. The details regarding the relative timing of sill

373   emplacement is poorly constrained and we thus use the same age for all sills. If the sills are closely spaced, this

374   will result in a higher maximum temperature in the sedimentary rocks between the sills (cf. (Aarnes et al.,

375   2011b)). For the erosion history of the Karoo Basin, we refer to Braun et al. (2014) and a rapid Late Cretaceous

376   erosion event.

5.2.1   Karoo KL1/78

378   The first example from the Karoo Basin is a short borehole with a length of 136 m that penetrates the Tierberg,

379   Whitehill and Prince Albert Formations. However, these Formations underlie a massive erosion sequence

380   consisting of 2.5 km of extrusives (Drakensberg Group) and 1.5 km of sediments (Stormberg and Beaufort

381   Groups) and are also included in the model. The borehole penetrates a single 15m thick sill at a depth of 72m

382   (Figure 10). The sill is emplaced within the Prince Albert Formation at 182.6 Ma at a temperature of 1150°C.

383   Initial average TOC data for the sedimentary layers is not known but can be roughly estimated using present-

384   day values. The initial TOC data is subsequently refined so that a better match of the model results to the

385   observed data is obtained, thereby highlighting how the model can be used to constrain initial conditions within

386   the sedimentary column (Figure 11). The importance of considering the entire basin history when constructing

387   the model is also emphasized by the VR results. The values of the VR results unaffected by the sill would be

388   much lower than the observed values if the eroded sequences are not considered. Addition of these layers to

389   the model results in added burial than would be expected than by just using the 136 m deep borehole. This

390   translates the VR curve laterally thereby better fitting the observed values (Figure 11). The final model shows a

391   good fit of TOC and VR to present day values. Model input data can be found in '1d_sill_input_kl178.xlsx'.

392
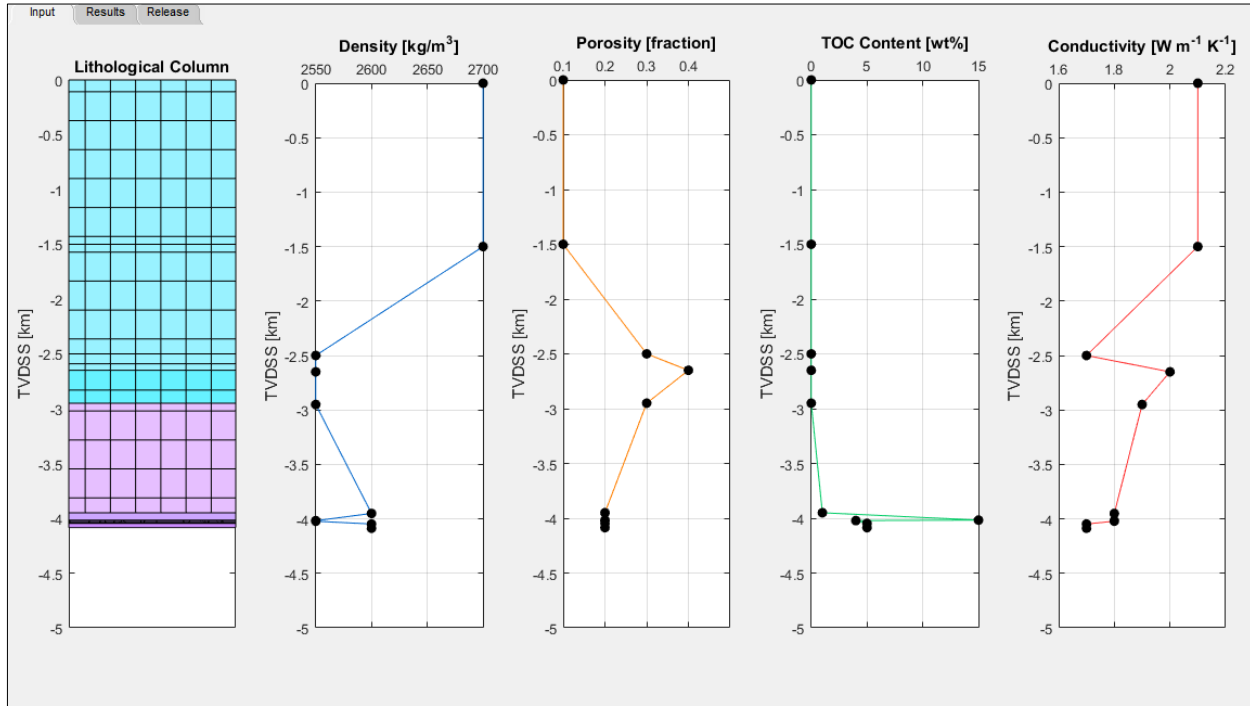
393

394   *Figure 8. Input tab for KL178.*

395
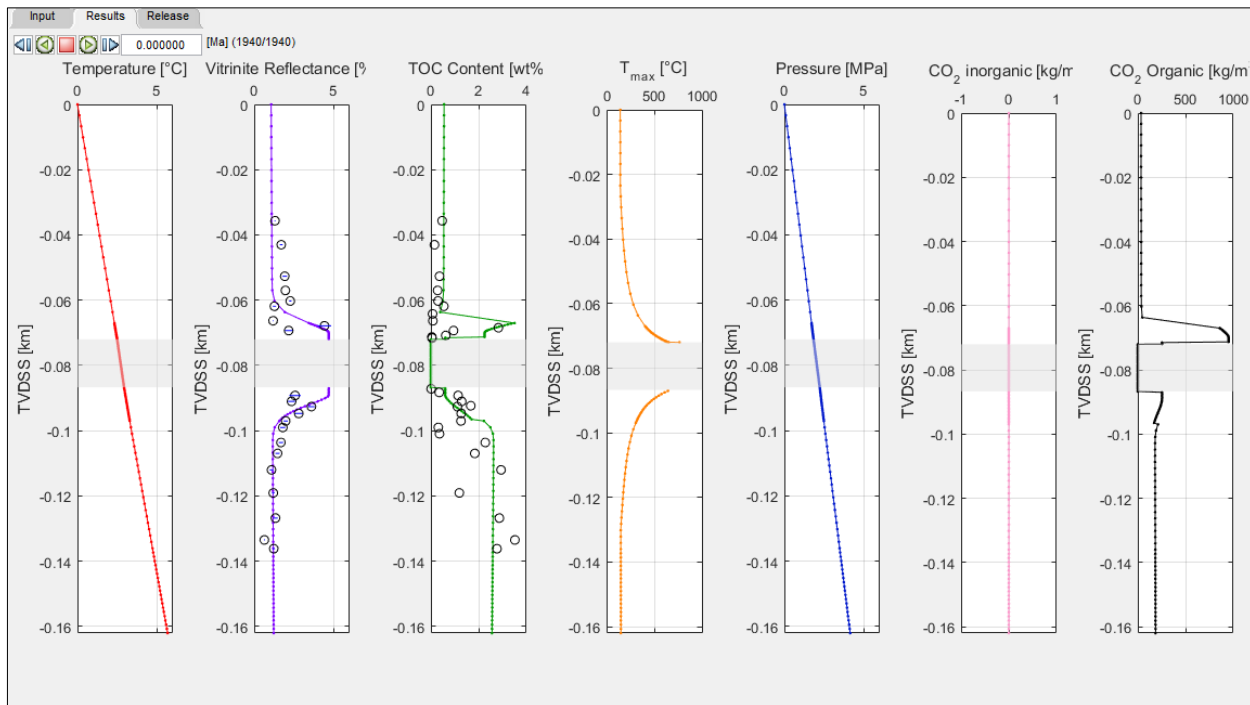
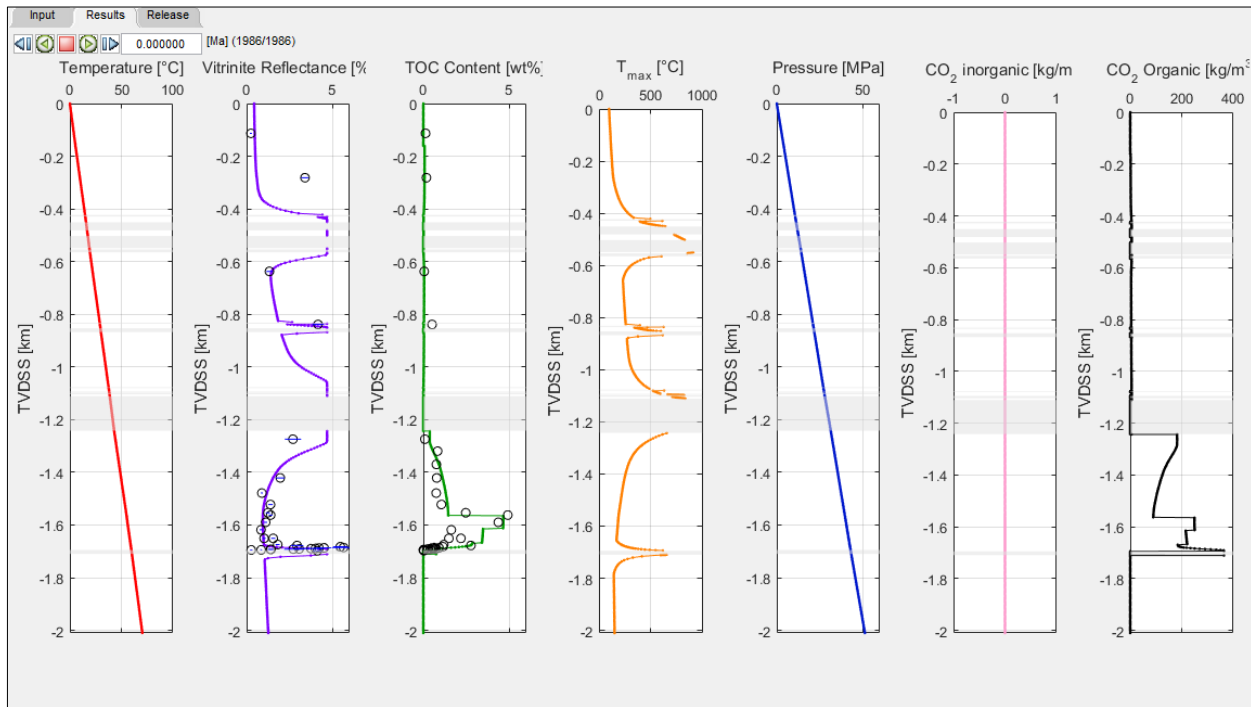*Figure 9. Results tab at the end of simulation time for KL178 shows a good match to present-day TOC and VR values.*

5.2.2 Karoo LA1/68

The second example from the Karoo Basin is a borehole with a length of 1711 m that penetrates the basin down to the basement (Svensen et al., 2015). Additional erosional sequence consisting mostly of the Drakensberg lavas and a minor section of the Stormberg Group is also added. The borehole penetrates multiple sills throughout the entire column with thicknesses ranging from 2 to 132m (Figure 10). Initial average TOC data for the sedimentary layers is estimated from present-day values. Similar to the previous example, material properties are iteratively changed within realistic bounds to arrive at an initial setup that matches the final observations well (Figure 11). Model input data can be found in '1d_sill_input_la168.xlsx'.
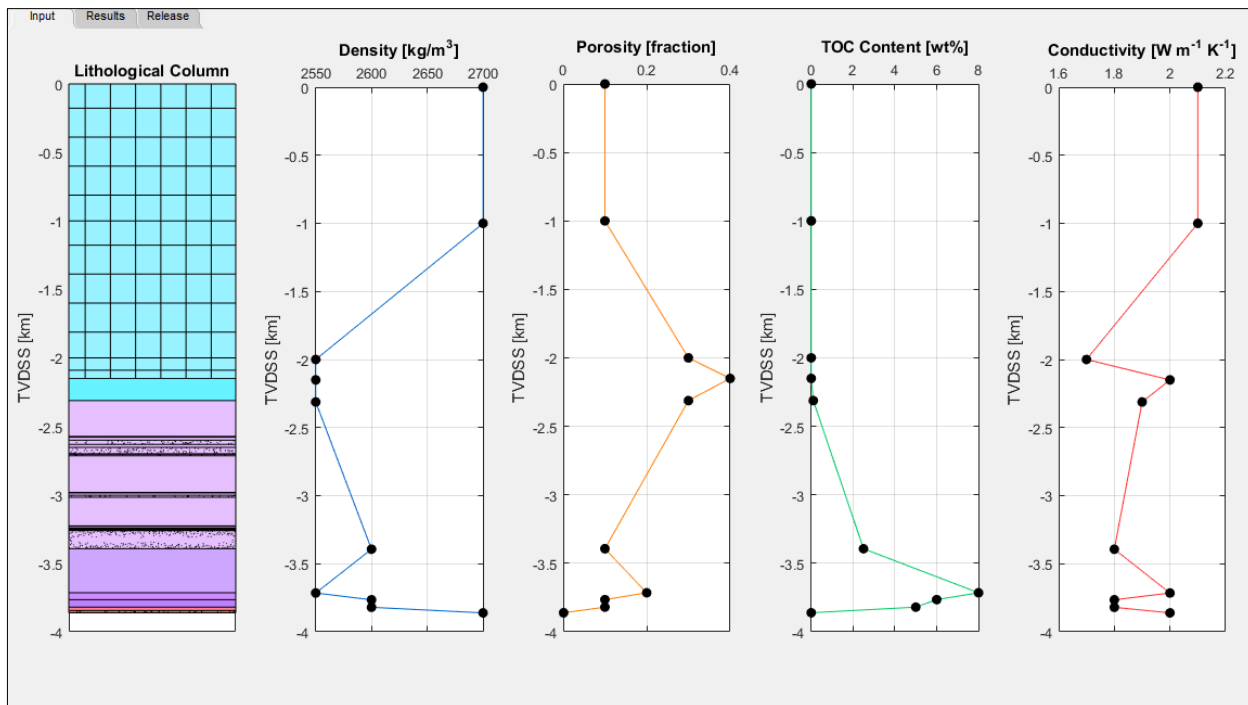
Figure 10. Input tab for LA168.

25

409

Figure 11. Results tab at the end of simulation time for LA168 shows a good match to present-day TOC and VR
values.

6   Conclusions

- SILLi is a numerical model quantifies the thermal evolution of contact aureoles around sills emplaced in sedimentary basins. The model includes basin history (burial and erosion), thus providing background-maturation levels of organic matter and consequently more realistic gas production estimates.

- SILLi is a user-friendly tool that is written in Matlab and uses Excel for input data.

- The 1D tool allows for the quick quantification of the thermal effects of sill intrusions. The results can be, therefore, used to further constrain and test the initial conditions that may have been present within the lithological column that match present-day observations.

- Model output includes peak temperature profiles, post-metamorphic TOC content, vitrinite reflectivity, and the cumulative amount and rate of CO_2 generation. These values can be readily upscaled to basin

423   scales if the sill extent is known. The amount of CO_2 can also be easily converted to other carbon-
424   bearing gases such as CH_4.

425 • Our three case studies demonstrate a good fit between aureole data (TOC and vitrinite reflectivity) and
426   model output showing that the model can be successfully applied to basins in various global settings.

427

7   Code Availability and Software Requirements

429   The source code with examples is archived as a repository on Github/Zenodo (DOI:
430   https://doi.org/10.5281/ZENODO.803748). Matlab 2014b or higher is required to run the code and Microsoft
431   Excel or any equivalent software is required to edit .xls files.

432

8   License (BSD-2-Clause)

449 The software includes errorbarxy.m by Qi An (2016) (BSD-2-Clause License)

450 (http://www.mathworks.com/matlabcentral/fileexchange/40221).

451

9   Author Contributions

453 K. Iyer and D.W. Schmid developed the code. K. Iyer implemented the code and wrote the manuscript. H.

454 Svensen guided code development and provided input data from field studies. D. W. Schmid and H. Svensen

455 edited the manuscript.

456

10   Competing Interests

458 The authors declare that they have no conflict of interest.

459

11   References

461 Aarnes, I., Fristad, K., Planke, S., and Svensen, H.: The impact of host-rock composition on devolatilization of
462 sedimentary rocks during contact metamorphism around mafic sheet intrusions, Geochem. Geophys. Geosyst.,
463 12, Q10019, 2011a.
464 Aarnes, I., Planke, S., Trulsvik, M., and Svensen, H.: Contact metamorphism and thermogenic gas generation in
465 the Vøring and Møre basins, offshore Norway, during the Paleocene–Eocene thermal maximum, Journal of the
466 Geological Society, doi: 10.1144/jgs2014-098, 2015. 588-598, 2015.
467 Aarnes, I., Svensen, H., Connolly, J. A. D., and Podladchikov, Y. Y.: How contact metamorphism can trigger global
468 climate changes: Modeling gas generation around igneous sills in sedimentary basins, Geochimica Et
469 Cosmochimica Acta, 74, 7179-7195, 2010.
470 Aarnes, I., Svensen, H., Polteau, S., and Planke, S.: Contact metamorphic devolatilization of shales in the Karoo
471 Basin, South Africa, and the effects of multiple sill intrusions, Chemical Geology, 281, 181-194, 2011b.
472 Braun, J., Guillocheau, F., Robin, C., Baby, G., and Jelsma, H.: Rapid erosion of the Southern African Plateau as it
473 climbs over a mantle superswell, Journal of Geophysical Research: Solid Earth, 119, 6093-6112, 2014.
474 Catuneanu, O., Hancox, P., and Rubidge, B.: Reciprocal flexural behaviour and contrasting stratigraphies: a new
475 basin development model for the Karoo retroarc foreland system, South Africa, Basin Research, 10, 417-439,
476 1998.
477 Chevallier, L. and Woodford, A.: Morpho-tectonics and mechanism of emplacement of the dolerite rings and
478 sills of the western Karoo, South Africa, S. Afr. J. Geol., 102, 43-54, 1999.
479 Connolly, J. and Petrini, K.: An automated strategy for calculation of phase diagram sections and retrieval of
480 rock properties as a function of physical conditions, Journal of Metamorphic Geology, 20, 697-708, 2002.

Geoscientific
Model Development
Discussions

481   du Toit, A. L.: the Karroo dolerites of south Africa: a study in hypabyssal injection, S. Afr. J. Geol., 23, 1-42, 1920.

482   Duncan, A., Erlank, A., Marsh, J., and Cox, K.: Regional geochemistry of the Karoo igneous province, 1984. 1984.

483   Fjeldskaar, W., Helset, H. M., Johansen, H., Grunnaleiten, I., and Horstad, I.: Thermal modelling of magmatic
484   intrusions in the Gjallar Ridge, Norwegian Sea: implications for vitrinite reflectance and hydrocarbon
485   maturation, Basin Research, 20, 143-159, 2008.

486   Galushkin, Y. I.: Thermal effects of igneous intrusions on maturity of organic matter: A possible mechanism of
487   intrusion, Organic Geochemistry, 26, 645-658, 1997.

488   Iyer, K., Rüpke, L., and Galerne, C. Y.: Modeling fluid flow in sedimentary basins with sill intrusions: Implications
489   for hydrothermal venting and climate change, Geochemistry, Geophysics, Geosystems, 14, 5244-5262, 2013.

490   Iyer, K., Schmid, D. W., Planke, S., and Millett, J.: Modelling hydrothermal venting in volcanic sedimentary
491   basins: Impact on hydrocarbon maturation and paleoclimate, Earth and Planetary Science Letters, 467, 30-42,
492   2017.

493   Jaeger, J.: Thermal effects of intrusions, Reviews of Geophysics, 2, 443-466, 1964.

494   Jaeger, J. C.: The temperature in the neighborhood of a cooling intrusive sheet, Am J Sci, 255, 306-318, 1957.

495   Jaeger, J. C.: Temperatures outside a cooling intrusive sheet, Am J Sci, 257, 44-54, 1959.

496   Jamtveit, B., Bucher-Nurminen, K., and Stijfhoorn, D. E.: Contact Metamorphism of Layered Shale-Carbonate
497   Sequences in the Oslo Rift: I. Buffering, Infiltration, and the Mechanisms of Mass Transport, Journal of
498   Petrology, 33, 377-422, 1992.

499   Jamtveit, B., Svensen, H., Podladchikov, Y. Y., and Planke, S.: Hydrothermal vent complexes associated with sill
500   intrusions in sedimentary basins. In: Physical Geology of High-Level Magmatic Systems, Breitkreuz, C. and
501   Petford, N. (Eds.), Geological Society Special Publication, Geological Soc Publishing House, Bath, 2004.

502   Kjoberg, S., Schmiedel, T., Planke, S., Svensen, H. H., Millett, J. M., Jerram, D. A., Galland, O., Lecomte, I.,
503   Schofield, N., and Haug, Ø. T.: 3D structure and formation of hydrothermal vent complexes at the Paleocene-
504   Eocene transition, the Møre Basin, mid-Norwegian margin, Interpretation, 5, SK65-SK81, 2017.

505   Lovering, T.: Theory of heat conduction applied to geological problems, Geological Society of America Bulletin,
506   46, 69-94, 1935.

507   Malthe-Sorenssen, A., Planke, S., Svensen, H., and Jamtveit, B.: Formation of saucer-shaped sills. In: Physical
508   Geology of High-Level Magmatic Systems, Breitkreuz, C. and Petford, N. (Eds.), Geological Society Special
509   Publication, Geological Soc Publishing House, Bath, 2004.

510   Monreal, F. R., Villar, H. J., Baudino, R., Delpino, D., and Zencich, S.: Modeling an atypical petroleum system: A
511   case study of hydrocarbon generation, migration and accumulation related to igneous intrusions in the
512   Neuquen Basin, Argentina, Marine and Petroleum Geology, 26, 590-605, 2009.

513   Moorcroft, D. and Tonnelier, N.: Contact Metamorphism of Black Shales in the Thermal Aureole of a Dolerite Sill
514   Within the Karoo Basin. In: Origin and Evolution of the Cape Mountains and Karoo Basin, Springer, 2016.

515   Pepper, A. S. and Corvi, P. J.: Simple kinetic models of petroleum formation. Part I: oil and gas generation from
516   kerogen, Marine and Petroleum Geology, 12, 291-319, 1995.

517   Planke, S., Rasmussen, T., Rey, S. S., and Myklebust, R.: Seismic characteristics and distribution of volcanic
518   intrusions and hydrothermal vent complexes in the Vøring and Møre basins. In: Petroleum Geology: North-
519   western Europe and global perspectives - Proceedings of the 6th Petroleum Geology Conference., Doré, A. G.
520   and Vining, B. A. (Eds.), Geological Society, London, 2005.

521   Svensen, H., Corfu, F., Polteau, S., Hammer, O., and Planke, S.: Rapid magma emplacement in the Karoo Large
522   Igneous Province, Earth and Planetary Science Letters, 325, 1-9, 2012.

Geoscientific
Model Development
Discussions

523   Svensen, H. and Jamtveit, B.: Metamorphic Fluids and Global Environmental Changes, ELEMENTS, 6, 179-182,
524   2010.
525   Svensen, H., Planke, S., Chevallier, L., Malthe-Sørenssen, A., Corfu, F., and Jamtveit, B.: Hydrothermal venting of
526   greenhouse gases triggering Early Jurassic global warming, Earth and Planetary Science Letters, 256, 554-566,
527   2007.
528   Svensen, H., Planke, S., Malthe-Sorenssen, A., Jamtveit, B., Myklebust, R., Rasmussen Eidem, T., and Rey, S. S.:
529   Release of methane from a volcanic basin as a mechanism for initial Eocene global warming, Nature, 429, 542-
530   545, 2004.
531   Svensen, H., Planke, S., Polozov, A. G., Schmidbauer, N., Corfu, F., Podladchikov, Y. Y., and Jamtveit, B.: Siberian
532   gas venting and the end-Permian environmental crisis, Earth and Planetary Science Letters, 277, 490-500, 2009.
533   Svensen, H. H., Planke, S., Neumann, E.-R., Aarnes, I., Marsh, J. S., Polteau, S., Harstad, C. H., and Chevallier, L.:
534   Sub-Volcanic Intrusions and the Link to Global Climatic and Environmental Changes, 2015. 2015.
535   Sweeney, J. and Burnham, A. K.: Evaluation of a simple model of vitrinite reflectance based on chemical kinetics,
536   AAPG Bulletin, 74, 1559-1570, 1990.
537   Tankard, A., Welsink, H., Aukes, P., Newton, R., and Stettler, E.: Tectonic evolution of the Cape and Karoo basins
538   of South Africa, Marine and Petroleum Geology, 26, 1379-1412, 2009.
539   Tracy, R. J. and Frost, B. R.: Phase equilibria and thermobarometry of calcareous, ultramafic and mafic rocks,
540   and iron formations, Reviews in Mineralogy and Geochemistry, 26, 207-289, 1991.
541   Walker, F. and Poldervaart, A.: Karroo dolerites of the Union of South Africa, Geological Society of America
542   Bulletin, 60, 591-706, 1949.
543   Wang, D. Y.: Comparable study on the effect of errors and uncertainties of heat transfer models on quantitative
544   evaluation of thermal alteration in contact metamorphic aureoles: Thermophysical parameters, intrusion
545   mechanism, pore-water volatilization and mathematical equations, International Journal of Coal Geology, 95,
546   12-19, 2012.
547   Wang, D. Y., Lu, X. C., Song, Y. C., Shao, R., and Qi, T. A.: Influence of the temperature dependence of thermal
548   parameters of heat conduction models on the reconstruction of thermal history of igneous-intrusion-bearing
549   basins, Computers & Geosciences, 36, 1339-1344, 2010.
550   Wang, D. Y. and Song, Y. C.: Influence of different boiling points of pore water around an igneous sill on the
551   thermal evolution of the contact aureole, International Journal of Coal Geology, 104, 1-8, 2012.
552   Wang, D. Y., Song, Y. C., Liu, Y., Zhao, M. L., Qi, T., and Liu, W. G.: The influence of igneous intrusions on the
553   peak temperatures of host rocks: Finite-time emplacement, evaporation, dehydration, and decarbonation,
554   Computers & Geosciences, 38, 99-106, 2012a.
555   Wang, K., Lu, X. C., Chen, M., Ma, Y. M., Liu, K. Y., Liu, L. Q., Li, X. Z., and Hu, W. X.: Numerical modelling of the
556   hydrocarbon generation of Tertiary source rocks intruded by doleritic sills in the Zhanhua depression, Bohai Bay
557   Basin, China, Basin Research, 24, 234-247, 2012b.